

Progress in Coupled Electron-Ion Monte Carlo Simulations of High-Pressure Hydrogen

Carlo Pierleoni

*Physics Department, University of L'Aquila,
L'Aquila, I-67010, Italy*

**E-mail: carlo.pierleoni@aquila.infn.it
www.fisica.aquila.infn.it*

Kris T. Delaney

*Materials Research Laboratory, University of California,
Santa Barbara, CA 93106-5121, USA*

E-mail: kdelaney@mrl.ucsb.edu

Miguel A. Morales, David M. Ceperley

*Physics Department, University of Illinois at Urbana-Champaign
Urbana, Illinois 61801, USA*

E-mail: mmorale@uiuc.edu, ceperley@uiuc.edu

Markus Holzmann

*LPTMC, Université Pierre et Marie Curie, 4 Place Jussieu, 75005 Paris, France
and*

LPMMC, CNRS-UJF, BP 166, 38042 Grenoble, France

E-mail: markus@lptmc.jussieu.fr

We report recent progress in the Coupled Electron-Ion Monte Carlo method and its application to high-pressure hydrogen. We describe the particular form of electronic trial wave functions that we have employed in applications for high-pressure hydrogen. We report wave function comparisons for static proton configurations and preliminary results for thermal averages.

Keywords: Quantum Monte Carlo; *Ab-initio* methods; High pressure hydrogen.

1. Introduction

Modern *ab initio* simulation methods for systems of electrons and nuclei mostly rely on Density Function Theory (DFT) for computing the electronic forces acting on the nuclei, and on Molecular Dynamics (MD) techniques to follow the real-time evolution of the nuclei. Despite recent progress, DFT suffers from well-known limitations.^{1,2} As a consequence, current *ab initio* predictions of metallization transitions at high pressures, or even the prediction of structural phase transitions, are often only qualitative. Hydrogen is an extreme case,³⁻⁵ but even in silicon, the diamond/ β -

tin transition pressure and the melting temperature are seriously underestimated.⁶

An alternative route to the ground-state properties of a many electrons system of is the Quantum Monte Carlo method (QMC).^{2,7} In QMC, a many-body trial wave function for the electrons is assumed and the electronic properties are computed by Monte Carlo methods. For fermions, QMC is a variational method with respect to the nodes of the trial wave function and a systematic, often unknown, error remains.^{2,7} Over the years, the level of accuracy of the fixed-node approximation has been improved⁸⁻¹¹ such that, in most cases, fixed-node QMC methods have proven to be more accurate than DFT-based methods, on one side, and less computationally demanding than correlated quantum-chemistry strategies (such as coupled cluster method)² on the other side. Computing ionic forces with QMC to replace the DFT forces in *ab initio* MD, poses additional problems whose solution has only very recently been proposed in a consistent way.^{12,13}

In recent years, we have been developing a different strategy, the Coupled Electron-Ion Monte Carlo (CEIMC) method, based entirely on Monte Carlo algorithms, both for solving the electronic problem and for sampling the ionic configuration space.¹⁴ The new method relies on the Born-Oppenheimer approximation. A Metropolis Monte Carlo simulation of the ionic degrees of freedom (represented either by classical point particles or by path integrals) at fixed temperature is performed based on the electronic energies computed during independent ground state Quantum Monte Carlo calculations. Application of CEIMC has so far been limited to high pressure hydrogen for several reasons: a) hydrogen is the simplest element of the periodic table, and the easiest to cope with since the absence of the additional separation of energy scales between core and valence electrons as in heavier elements; b) it is an important element since most of the matter in the universe consists of hydrogen; c) its phase diagram at high pressure in the interesting region where the metallization occurs is still largely unknown because present experiments are not able to reach the relevant pressures. We have investigated the very high pressure regime where all molecules are dissociated and the system is a plasma of fully ionized protons and electrons,¹⁵ and we have studied the pressure-induced molecular dissociation transition in the liquid phase.¹⁶ In both studies the CEIMC results were not in agreement with previous Car-Parrinello Molecular Dynamics (CPMD) calculations.^{17,18} While we have evidence now that the discrepancy in the fully ionized case is removed by taking our new more accurate trial wave function, in the second study more accurate CEIMC calculations predict a continuous molecular dissociation with increasing pressure at variance with CPMD where a first order molecular dissociation transition was observed by increasing pressure at constant temperature. Recently, using constant volume Born-Oppenheimer Molecular Dynamics rather than constant pressure CPMD, a continuous dissociation transition has been reported from DFT-GGA studies¹⁹

In the present paper we will discuss in some details the various trial wave functions we have implemented for hydrogen. In Section 2 we briefly review the basic ingredients of the method. Section 3 will be devoted to describing the different trial

wave functions and some details on their efficient implementation. In Section 4 we will report numerical comparisons among the various trial functions. Finally, in Section 5 we collect our conclusions and perspectives.

2. The CEIMC Method

In this section we briefly outline the basic ingredients of the CEIMC approach. Further details can be found in several published reviews.^{14,20,21}

CEIMC, in common with the large majority of *ab-initio* methods, is based on the Born-Oppenheimer separation of “slow” ionic degrees of freedom and “fast” electronic degrees of freedom. In addition, the electrons are considered to be in their ground state which depends on the instantaneous proton positions. Protons, either considered as classical or quantum particles, are assumed to be at thermal equilibrium with a heat bath at fixed temperature T . The system of N_p protons and $N_e = N_p$ electrons is enclosed in a given volume V which provides a fixed number density $n = N_p/V$, better expressed in terms of the coupling parameter $r_s = (3/4\pi n)^{1/3}$.

The thermal equilibrium distribution of proton states S , $P(S) \propto e^{-\beta E_{BO}(S)}$ is sampled by a Metropolis Monte Carlo calculation.²² Here S is the $3N_p$ -dimensional vector of proton positions and $E_{BO}(S)$ the corresponding Born-Oppenheimer energy defined as $E_{BO}(S) = \langle \Phi_0(S) | \hat{H} | \Phi_0(S) \rangle$ where \hat{H} is the hamiltonian of the system and $|\Phi_0(S)\rangle$ its ground state. In order to compute an estimate of $E_{BO}(S)$ we employ both Variation Monte Carlo (VMC) and Reptation Quantum Monte Carlo (RQMC)²³ methods within the “fixed node” (for real trial functions) or “fixed phase” (for complex trial functions) approximation.^{2,14} The bounce algorithm for sampling the electronic paths within RQMC is implemented.^{14,24}

The estimate of $E_{BO}(S)$ for a given trial function computed by QMC is affected by statistical noise which, if ignored, will provide a biased sampling. The size of the bias increases for increasing noise level. A possible solution would be to run very long QMC calculations in order to get a negligibly small noise level, and thus a negligible bias. However, for each protonic configuration S , the noise level decreases as the square root of the number of independent estimates of $E_{BO}(S)$. This means that in order to decrease the noise level by one order of magnitude we should generate 100 times more uncorrelated samples, an unfavorable scaling especially given that the process must be repeated for any attempted move of the ions. The less obvious, but far more efficient, solution is to generalize the Metropolis algorithm to noisy energies. One such algorithm is the Penalty Method.^{14,25} The idea is to require the detailed balance to hold on average (over the noise distribution) and not for a single energy calculation. Within the Penalty Method the acceptance probability of a single protonic move $S \rightarrow S'$ depends, not only on the energy difference between the two states $\beta[E_{BO}(S') - E_{BO}(S)]$, but also on the noise of the energy difference $(\beta\sigma)^2$. Here β is the inverse physical temperature of the protons. Since $(\beta\sigma)^2 > 0$ the presence of the noise always causes extra rejection of attempted moves with respect

to the noiseless case. It is clear that the method is successful if one can allow for a large and cheap noise level still keeping a nonvanishing acceptance probability (≤ 0.1). A rule of thumb for maximum efficiency is to have $(\beta\sigma) \sim 1$.²⁵ An efficient energy difference method is exploited to compute the energy difference and its noise.^{14,20}

A well known problem for QMC energies, in particular for metals, is caused by finite size effects, mainly coming from the discrete nature of the reciprocal space of finite and, generally small, systems. For a degenerate Fermi liquid, finite-size shell effects are much reduced if twist averaged boundary conditions (TABC) are used.²⁶ For a given property \hat{A} , the TABC is defined as

$$\langle \hat{A} \rangle = \int_{-\pi}^{\pi} \frac{d\vec{\theta}}{(2\pi)^d} \langle \Psi_{\vec{\theta}} | \hat{A} | \Psi_{\vec{\theta}} \rangle \quad (1)$$

where $\vec{\theta}$ is a 3D-vector specifying the undetermined phase that the N -body wave function $\Psi_{\vec{\theta}}(\vec{r}_1 + L\vec{n}, \vec{r}_2, \dots) = e^{i\vec{\theta}} \Psi_{\vec{\theta}}(\vec{r}_1, \vec{r}_2, \dots)$ picks up when a particle wraps around the boundary of the simulation box.

TABC is particularly important in computing properties that are sensitive to the single particle energies, such as the kinetic energy and the magnetic susceptibility. By reducing shell effects, accurate estimates of the thermodynamic limit for these properties can be obtained already with a limited number of electrons.

In CEIMC, we can take advantage of twist averaging to reduce the noise in the energy difference for the acceptance test of the penalty method. Different strategies can be used to implement the TABC. One possibility is to use a fixed 3D grid in the twist angle space, at each grid point run independent QMC calculations and then average the resulting properties. However, the optimal noise level in CEIMC is $\beta\sigma \sim 1$ and a limited number of twists are able to satisfy this requirement at high temperature. At the same time, too coarse a grid introduces a systematic effect on the energy of the system. To illustrate this fact we report in panel a) of figure 1 for a single pair of configurations of 16 protons at $r_s = 1$ and $T = 3000K$, the energy difference as obtained with VMC and the metallic wave function (see Section 3). The energy difference is indeed the key quantity in CEIMC since it guides the Metropolis sampling of the protonic degrees of freedom. As can be seen, the energy difference computed over a fixed grid has an oscillating behavior with the number of twists, which implies that convergence requires a large numbers of twists. Running that large number of twists will be very time consuming and will provide a noise level much smaller than the optimal value. To solve this problem of efficiency, we can think of the twist angle as an additional random variable to be sampled during the protonic MC simulation. To this aim, we still use a fixed grid in the twist-angle space, but at each protonic step we sample a value of the twist angle inside the Wigner-Seitz cell around each grid point. In panel a) of figure 1, we also report the value of the energy difference obtained sampling the twists for the same pair of proton configurations. We see that the energy difference converge much more rapidly with the number of the twists, as expected. The conclusive test on the accuracy of

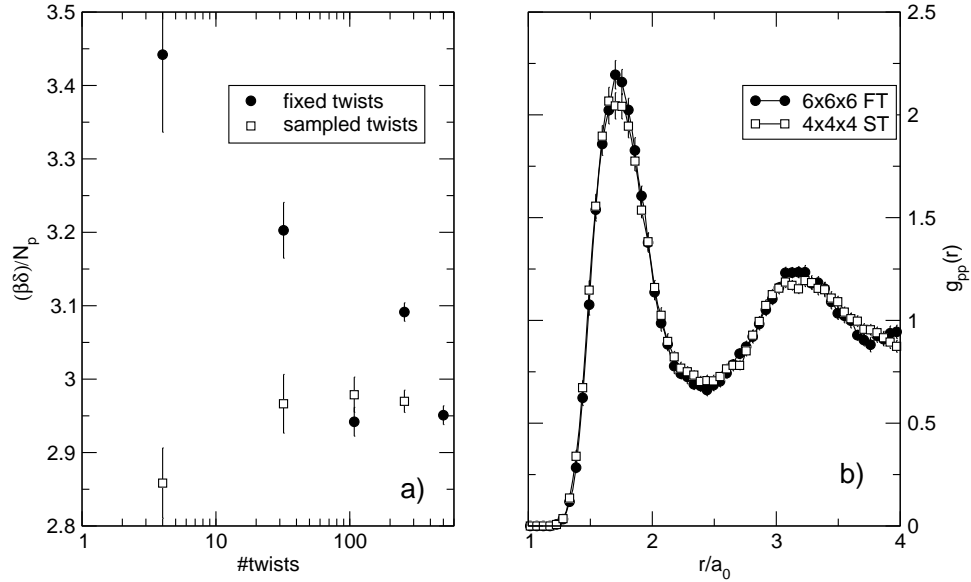


Fig. 1. a) Reduced energy difference for a pair of protonic configurations of a 16 protons system at $r_s = 1$ sampled during a run at $T = 3000K$ versus the number of twist angles. The energy difference is obtained with the metallic trial function and at the VMC level. Closed circles corresponds to fixed twists on a Monkhorst-Pack grid with $2 \times 2 \times 2$, $4 \times 4 \times 4$, $6 \times 6 \times 6$, $8 \times 8 \times 8$ and $10 \times 10 \times 10$ (with inversion symmetry), while squares corresponds to twists sampled as explained in the text. b) proton-proton pair correlation function for a system of 54 protons at $r_s = 1$ and $T = 1500K$ with the metallic trial function at the VMC level. Closed circles are data for fixed twists on a $6 \times 6 \times 6$ grid while squares are for 32 sampled twists.

the twist sampling is, however, provided only by comparing equilibrium CEIMC calculations with fixed and sampled twists. This is illustrated in panel b) of figure 1 for 54 protons at $r_s = 1$ and $T = 1500K$, comparing the the proton-proton pair correlation functions obtained by using 108 fixed twists and 32 sampled twists at the VMC level and with the metallic wave function (see Section 3).

3. Trial Wave Functions for Hydrogen

In the first implementation of CEIMC,^{20,21} our goal was to simulate the insulating phases of molecular hydrogen and, as such, a trial function consisting of a few optimizable gaussian molecular orbitals centered on each molecule was used. Optimization of the variational parameters, in number proportional to the number of electron in the system, needed to be performed at each ionic configuration and was a major bottleneck for the efficiency of the method. Subsequently, we have developed trial functions with a very limited number of variational parameters (even zero when possible) and therefore reduce the complexity of the optimization step in the electronic calculation (or to reduce to a linear optimization in the case of DFT orbitals). In Ref.¹⁰ we have shown, as the Feynman-Kac formula suggests, a

procedure to iteratively improve any initial trial function. If a Hartree-Fock (HF) determinant is assumed as an initial ansatz, the first iteration generates a bosonic (symmetric) two-body correlation function (Jastrow) while the next iteration naturally provides the backflow transformation of the orbitals and a three-body bosonic correlation term. Unfortunately, this is a formal theory which cannot provide, in general, analytical expressions for the various terms. Nonetheless the general structure is illuminating in searching for improvements.

3.1. *The Metallic Wave Function*

At a very high pressure, beyond metallization and molecular dissociation, the electron liquid is a good Fermi liquid and correlation effects, with protons and among electrons, can be treated as perturbations. In this case it is natural to assume a determinant of free electron states (plane waves) as an initial ansatz. An accurate and parameter free Jastrow factor can be obtained within the RPA $u_{ij}^{RPA}(r)$ ($i, j = e, p$).²⁷ This simple form satisfies the correct cusp conditions at short particle separations and the right plasmon behavior (screening) at large distances. It was shown²⁸ to provide good energies for hydrogen even at intermediate densities if supplemented by gaussian functions $\tilde{u}_{ij}(r) = u_{ij}^{RPA}(r) - \alpha_{ij} e^{-r^2/w_{ij}^2}$, with the variational parameters α_{ij}, w_{ij} . The additional term preserves the short- and long-distance behavior of the RPA function and corrects for possible inaccuracies at intermediate distances. However, they introduce four variational parameters, namely $\alpha_{ee}, w_{ee}, \alpha_{ep}, w_{ep}$. As stated above, the next iteration suggests the backflow transformation of the orbitals and a three-body correlation factor. This is a crucial step for an inhomogeneous electron system, since the nodal surfaces of the trial wave function will become explicitly dependent on the proton positions and will provide a more accurate energy even at the RQMC level. Similar to the case of the homogeneous electron gas,⁹ the backflow and three-body functions were at first parametrized as gaussians.²⁰ This trial function has a total of 10 free parameters to be variationally optimized and has been used in a first CEIMC study of the melting transition of the proton crystal in hydrogen at $r_s = 1$.²⁰ Next, we were able to derive approximate analytical expressions for the backflow and the three-body functions, as well as for the two-body correlation factor, in the Bohm-Pines collective coordinates approach.¹⁰ This form is particularly suitable for the CEIMC because it is parameter-free. At the same time, it provides comparable accuracy to the numerically optimized wave function, both in the crystal configuration and for disordered protons (see Section 3.2). Explicit forms of the various terms can be found in the appendix of Ref.¹⁰ With this kind of wave function we have investigated the melting at three densities ($r_s = 0.8, 1.0, 1.2$) including quantum effects for protons.^{14,15}

3.2. *Band-structure-based Wave Functions (IPP/LDA)*

The metallic wave function is expected to provide an accurate description of the electronic ground state at high density, well beyond molecular dissociation and

metallization. On the other hand we expect it to be a poor representation of the true ground state at lower densities where molecules appear and plane-wave single-electron orbitals (although in terms of backflow coordinates) are certainly not a good representation. Natoli *et al.*^{29,30} have previously used a Slater determinant of Kohn-Sham self consistent orbitals to study the solid phases of atomic hydrogen at $r_s = 1.31$ and $T = 0$, and of molecular hydrogen at lower densities. They have found a typical energy gain of 0.5eV/electron by replacing the plane-wave with the self consistent orbitals in the Slater determinant. Here we have implemented similar ideas. The single-particle orbitals, $\{\phi_n\}$, that comprise the Slater determinant are computed on-the-fly during the CEIMC calculation as the eigenstates of some single-particle Hamiltonian,

$$\hat{h}\phi_n(\mathbf{r}) = \left[-\frac{1}{2}\nabla^2 + V_{\text{eff}}(\mathbf{r}; S) \right] \phi_n(\mathbf{r}) = \varepsilon_n \phi_n(\mathbf{r}), \quad (2)$$

where the $N/2$ orbitals with the lowest eigenvalue, ε_n , are selected to fill the determinants. The single-particle Hamiltonian \hat{h} describes electron-nuclear interactions and approximates electron-electron interactions through an effective potential.

To solve the eigenvalue problem we use an iterative, conjugate-gradients band-by-band minimization scheme.³¹ The method employs the variational principle to minimize residuals, and the Gram-Schmidt scheme to preserve orthogonalization of the eigenstates.

In our studies, we assume either $V_{\text{eff}} = V_{e-n}$, the bare electron-nuclear interaction (IPP independent particle potential), or $V_{\text{eff}} = V_{\text{LDA}}$, the Kohn-Sham effective potential within the local density approximation (LDA) with the Perdew-Zunger³² parameterization of Ceperley-Alder³³ electron-gas data. In both cases, the wave functions are eigenstates of a Hamiltonian which contains a bare Coulomb interaction between electrons and protons. The singularity in the potential results in a derivative cusp in the orbitals $-\partial \ln[\phi(\mathbf{r})]/\partial \mathbf{r} = 1$ for $\mathbf{r} = \mathbf{R}_I$. This cusp is important for obtaining good energies or short projection times for QMC algorithms. Representing this cusp on a plane wave basis is challenging due to the slow algebraic decay of k^{-4} . For this reason, we implement a cusp-removal method by dividing the orbitals by a function that satisfies the cusp condition exactly (in this case, the RPA *ep* Jastrow function discussed earlier), before reverse Fourier transforming to retrieve the plane wave coefficients of the orbitals used to build the Slater determinant. The proper electron-proton cusp is later reintroduced using the same RPA Jastrow function. This procedure greatly enhances the convergence of the Slater-Jastrow wave function with respect to the size of the plane-wave basis set used to represent the orbitals

3.3. Backflow Transformations of IPP/LDA Orbitals

Further complexity may be introduced into these trial functions through the use of a backflow transformation which introduces correlations into the fermionic part of a Slater-Jastrow wave function, with the advantage that modifications of the

nodal surface are possible. As previously discussed, analytic forms for the backflow function have been derived using the Bohm-Pines collective coordinates approach.¹⁰ While this form is strictly valid for plane-wave states in a determinant, we could think of applying the Feynman-Kac iteration to generate a backflow transformation even for IPP or LDA orbitals. The specific form for the transformation is unknown, but as a first ansatz we can use the same expressions we have developed in the metallic case. The obtained trial functions will be denoted IPPBF and LDABF respectively. As we will show in the next section, this procedure is found always to improve the total energy and its variance, providing therefore a better representation of the ground state of the system.

4. Comparisons of Wave Functions

4.1. *Fixed protons configurations*

In this section we consider fixed proton configurations and we compare the quality of the various wave functions at two densities, corresponding to $r_s = 1.0$ and $r_s = 1.4$. Results for hydrogen at $r_s = 1.31$ in the BCC structure obtained from various improvements of the metallic wave function are reported in Table III of Ref.¹⁰ where they are also compared to the results obtained with self-consistent Kohn-Sham orbitals.²⁹ There we have shown that the quality of the analytical form of the metallic wave function is superior to its numerically optimized version and comparable to that of the LDA orbitals for hydrogen in the BCC structure and for various system sizes. Our present implementation of LDA orbitals provides results in agreement with previous estimates.³⁴

In Table 1 we report QMC energies for hydrogen in several crystal structures and for various system sizes. A complete study of the size dependence and the relative stability of those structure is not our concern here and will be reported elsewhere.³⁴ From Table 1 we observe that LDA always provides a small or negligible improvement over IPP, while IPP is significantly cheaper through the lack of the self-consistent requirement. Comparing various structures and system sizes, we observe that the best wave function depends on the structure: for BCC, FCC structures and the diamond structure with $N=8$, the metallic wave function is superior to the others. The opposite is true for the diamond structure with $N=64$, where IPP and LDA provide lower energies at all densities. We also observe that the ordering of wave functions does not appear to depend on density, at least in the limited range investigated. Note that $r_s = 1.31$ corresponds to the density predicted by ground state QMC calculations²⁸ for the molecular dissociation to occur. Another important test is the effect of backflow (BF) on the band orbitals. We see that both at the variational and at the reptation level the energy is slightly improved and at the same time the variational variance is halved by the backflow, which means a net improvement of the variational function and the need of a shorter projection in imaginary time to reach the ground state. The high level of accuracy observed for the metallic wave function induced us to perform a detailed study of liquid hydrogen

Table 1. The energy and variance of hydrogen in various structures with different trial functions. All results are obtained averaging over a 6x6x6 fixed grid of twist angles. E_v and σ_v^2 represent, respectively, energy and variance at the variational level while E_r and σ_r^2 are the energy and the mixed estimator for the variance obtained with RQMC. Units are Hartree/atom.

		$r_s = 1.0$				$r_s = 1.4$				
		WFS	E_v	σ_v^2	E_r	σ_r^2	E_v	σ_v^2	E_r	σ_r^2
$(N_p = 54)$	Met		-0.36931(1)	0.0279(2)	-0.3721(1)	0.0182(7)	-0.5203(2)	0.036(2)	-0.5224(1)	0.01008(4)
	IPP				-0.3681(3)	0.0765(3)	-0.5139(1)	0.0887(2)	-0.5209(2)	0.0284(1)
	LDA				-0.3681(2)	0.0765(2)	-0.5145(1)	0.0869(3)	-0.5210(2)	0.0286(1)
	IPP+BF				-0.3705(1)	0.0359(1)			-0.5228(1)	0.01413(7)
	LDA+BF		-0.36805(2)	0.04636(4)	-0.3705(1)	0.0357(1)				
$(N_p = 32)$	Met				-0.3792(1)	0.01543(4)			-0.5272(1)	0.00872(3)
	IPP				-0.3756(2)	0.0756(2)	-0.5210(1)	0.0835(3)	-0.5256(1)	0.0276(1)
	LDA				-0.3757(2)	0.0753(2)	-0.5212(1)	0.0828(3)	-0.5259(1)	0.02724(9)
	IPP+BF				-0.3779(1)	0.03550(9)			-0.5280(1)	0.01352(5)
	LDA+BF				-0.3779(1)	0.0351(1)				
$(N_p = 64)$	Met				-0.3477(2)	0.0268(1)			-0.5168(1)	0.01656(8)
	IPP				-0.3621(2)	0.0830(4)	-0.5189(2)	0.1027(8)	-0.5321(5)	0.0339(3)
	LDA				-0.3613(2)	0.0823(3)			-0.5323(1)	0.0331(2)
	IPP+BF				-0.3637(1)	0.0404(1)			-0.5346(1)	0.01740(7)
	LDA+BF				-0.3635(1)	0.0406(1)				
$(N_p = 8)$	Met		-0.41060(4)	0.02136(4)	-0.41368(6)	0.01032(2)				
	IPP		-0.40198(8)	0.0863(1)	-0.4094(1)	0.04342(8)				
	LDA		-0.40206(8)	0.0865(1)	-0.4098(1)	0.04356(6)				
	IPP+BF		-0.40632(6)	0.04958(8)	-0.41070(6)	0.02382(4)				
	LDA+BF		-0.40638(6)	0.04958(8)	-0.4107(1)	0.02382(6)				

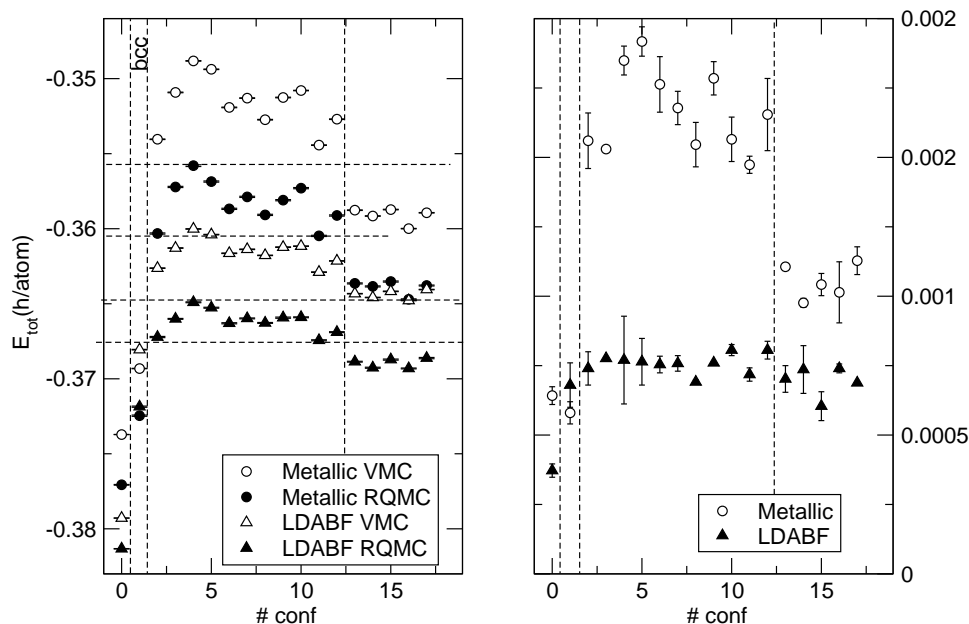


Fig. 2. Total energy (left panel) and quality parameter (right panel) for a number of static proton configurations as obtained with the metallic and the LDABF trial functions at $r_s = 1$. TABC with a $6 \times 6 \times 6$ fixed grid in the twist space is performed. Energies are in h/atom.

at finite temperature.¹⁵

Next, we consider how the various wave functions perform on disordered protonic configurations representative of atomic hydrogen in the liquid state. As before, all results reported here are averaged over a $6 \times 6 \times 6$ fixed grid in the twist space. At $r_s = 1$ we compare the Metallic wave function with the LDABF wave function, while at lower density we report data for the IPP, IPPBF and the LDABF wave functions. Data for configurations at $r_s = 1$ are presented in Figure 2. We display on the left panel VMC and RQMC energies for 18 protonic configurations obtained with the metallic and the LDABF wave functions. Configuration 0 is a 32 protons warm crystal near melting (FCC), configuration 1 is the perfect BCC crystal with 54 protons, configurations 2 to 12 are statistically independent configurations of 54 protons obtained during a CEIMC run at $T=2000\text{K}$ performed with the LDABF trial function, while the remaining 5 configurations have been obtained during a CEIMC run at the same temperature performed with the metallic trial function. The panel on the right reports the values of the quality parameter^a. Several interesting facts can be inferred from this figure. With the noticeable exception of the

^aThe quality parameter of a trial function is defined as the negative logarithm of the overlap of the trial state onto its fully projected state. It is easy to prove that it reduces to the integral over the positive imaginary time axis of the difference between the energy and its extrapolation at infinite time. The smaller the quality parameter the better the trial function is.

perfect BCC crystal, energies from LDABF wave function are always lower than energies from the metallic wave function. In particular, the fully converged RQMC energies from the metallic wave functions are above the VMC energies from LDABF. This implies that changing the form of the nodes provides more energy than fully projecting the initial state. Why the excellent quality of the metallic wave function observed in perfect crystals is deteriorated by disordered remains unclear to us, but as a matter of fact it appears that LDA nodes supplemented by e-e backflow perform much better both in the liquid state and in the crystal state with thermal fluctuations. Another interesting observation concerns the dispersion of the energies over a set of configurations. Let us consider the first 11 liquid configurations (from 2 to 13) generated during a run with the LDABF trial function. Considering the RQMC energies, the dispersion is 4.68(4) mH/atom with the metallic wave function but only 2.54(4) mH/atom with the LDABF wave function (see horizontal dashed lines in the left panel of Figure 2), that is the BO surface with LDABF is smoother than the other and the liquid will be less structured (see the next section). Finally, it is interesting to compare the dispersion of the VMC and the RQMC energies for a given trial function and a given set of configurations. Always for the first 11 liquid configurations and for the LDABF wave function we have 2.88(4) mH/atom at the VMC level versus 2.54(2) mH/atom at RQMC level. This implies that projecting the trial wave function will only provide a tiny difference in the roughness of the BO energy surface (corresponding to a temperature effect of $\sim 0.34mH/atom = 100K$). As for the quality parameter, we similarly observe that, with the exception of the BCC crystal, the metallic wave function has larger values, which means that it is less accurate than the LDABF wave function. Note also, how the quality of the LDABF wave function is uniform (at fixed number of particles) through the perfect crystal and the disordered configurations, no matter how these configurations have been generated. This is an important requirement to accurately predict phase transitions. On the other hand, the quality of the metallic wave function on the 5 liquid configurations generated with this wave function is higher than on the remaining 10 liquid configurations generated in a LDABF run. A good trial function should have a uniform quality throughout the entire proton configurational space in order to provide an unbiased sampling. A similar analysis has been performed at $r_s = 1.4$ considering 5 uncorrelated liquid configurations generated during a CEIMC run at $T = 2000K$ with the LDABF trial function. Results are displayed in Figure 3. Since the metallic wave function is certainly not accurate at this density, we compare the IPP and LDABF wave functions only. Again, the quality of LDABF is superior to the quality of the other wave function because it has a lower energy (its VMC energy is very close the RQMC-IPP energy) and a smaller and more uniform quality parameter. As for the dispersion of the energy at the RQMC level we obtain 10.9(2) mH/atom for LDABF and 13.3(2) mH/atom for IPP suggesting that the liquid structure at a given temperature (and in particular the molecular fraction) could depend considerably on the trial functions. Finally the VMC and RQMC energy dispersions for LDABF are 11.1(1)mH/atom and 10.9(2)mH/atom

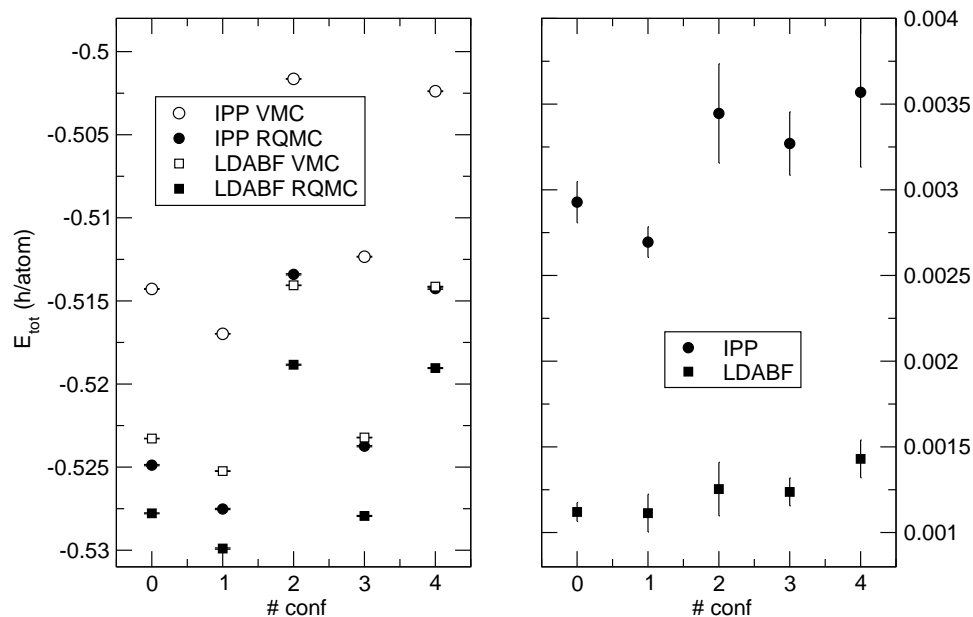


Fig. 3. Total energy (left panel) and quality parameter (right panel) for a number of static proton configurations as obtained with the metallic and the LDABF trial functions at $r_s = 1.4$. TABC with a $6 \times 6 \times 6$ fixed grid in the twist space is performed. Energies are in h/atom.

respectively, suggesting, as before, that projecting the trial wave function will only slightly change the protonic structure, the larger effect being in changing the nodal structure.

4.2. Liquid-State Simulations

After the validation of LDABF trial function of the previous section, we report here results for the liquid structure of hydrogen at the same densities. We have simulated systems of 54 protons. The TABC is performed here using twist sampling around the nodes of a $4 \times 4 \times 4$ grid in twist space at each protonic step. In the left panel of Figure 4 we report a comparison of proton-proton pair correlation functions $g_{pp}(r)$ at $r_s = 1$ and $T = 1500K$ as obtained from the metallic and LDABF trial functions at the VMC level. As expected from the results of the previous section, we observe considerably more structure with the metallic trial function than with the LDABF one, which indeed would correspond to having an effective lower temperature. On the same figure we report results from a CPMD simulation¹⁷ performed within the LDA approximation. The agreement between CPMD data and our present CEIMC data from LDABF trial function is striking and somehow unexpected. Indeed our representation of the electronic ground state is much more accurate than the simpler LDA one. Also the finite size effect in the CPMD calculation was addressed only partially by using only closed shells systems at the Γ point. Nonetheless the observed

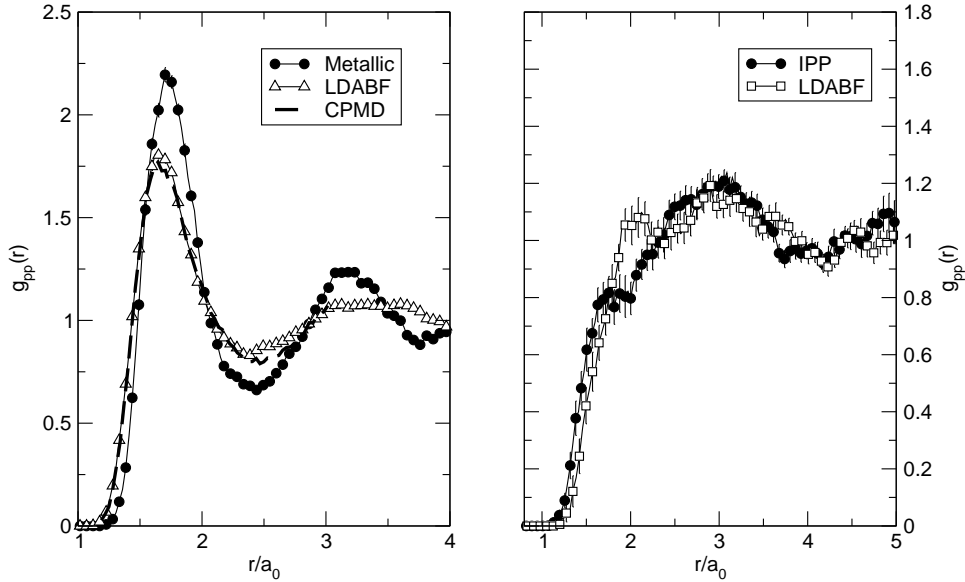


Fig. 4. Left panel: $r_s = 1, T = 1500K, N_p = 54$. Proton-proton pair correlation functions as obtained with LDABF and metallic wave functions. Results are obtained with TABC by using twist sampling around a $4 \times 4 \times 4$ grid. CPMD data from ref.¹⁷ are also represented by a thick dashed line. Right panel: $r_s = 1.4, T = 2000K, N_p = 54$. Proton-proton pair correlation functions as obtained with IPP and LDABF trial functions as obtained with TABC by using a $6 \times 6 \times 6$ fixed grid (IPP) and by twist sampling around a $4 \times 4 \times 4$ grid (LDABF).

agreement testify that the structure of the proton liquid is not very sensitive to details of the ground state representation. Finally, in the right panel of Figure 4 we report preliminary data for $g_{pp}(r)$ of 54 protons at $r_s = 1.4$ and $T = 2000K$. We compare IPP and LDABF trial functions at the VMC level. The statistical noise is still large but it seems that the overall behavior does not depend too much on the kind of trial functions, although small details could still be different. Note, however, that the liquid has little structure. More investigations of the influence of the trial function on the liquid structure is certainly needed, in particular, in the molecular dissociation region.

5. Conclusions

We have reported important progress in CEIMC, an efficient and accurate method to perform *ab-initio* simulations of condensed system with QMC energies. We have shown how the method performs in the case of hydrogen at high pressure, the simplest, but yet not understood, system. The new method allows us to cover a range of temperatures inaccessible to previous QMC methods for hydrogen, a range where most of the interesting physics of hydrogen occurs, including the melting of the molecular and proton crystals, the molecular dissociation both in the liquid and

in the crystal and the metallization of the system.

A key ingredient in CEIMC is the trial function used to represent the electronic ground state. Even when a projection technique such as Reptation QMC is exploited to improve the bosonic part of the trial many-body wave function, its fermionic part, that is its nodal surface, is still playing a very crucial role in determining the electronic energies and therefore the overall thermal behavior of the system. In the present paper, we have reported a detailed investigation of these effects for hydrogen by comparing a number of different trial wave functions at two densities. We have shown as a fully analytical trial wave function, that is optimal in terms of computational efficiency in CEIMC, and which has been previously demonstrated to provide excellent accuracy for crystalline states, degrades as soon as some disorder is introduced in the protonic configurations. This result has been established by comparing with results for new trial functions obtained from a Slater determinant of IPP/LDA orbitals together with a two-body Jastrow correlation factor. A further backflow transformation of these orbitals has been introduced and characterized. The new trial functions provide lower energies and more uniform overlap over a number of fixed representative configurations, which we use as an indication of the overall quality of the trial function. The most striking result on disordered configurations is that the LDABF energies at the VMC level are lower than the fully projected energies from the metallic trial function. This indicates that the improvement of performance comes mainly from the different nodal surfaces, while the bosonic part is responsible only for smaller improvements. The failure of the metallic wave function is most probably due to the presence of some degeneracy of its orbital structure around the Fermi surface which is removed by solving the instantaneous band structure. On the other hand, the use of complex wave functions and twist averaged boundary conditions in connection with the metallic trial function was expected to remove most of these degeneracies. A better understanding of this failure is desirable and deserves more investigation.

The difference in energies for different trial functions, or more precisely the dispersions of the energies from different wave functions, translates in a overall temperature factor at thermal equilibrium. The metallic trial function provides a dispersion which is roughly twice that of the corresponding dispersion from the LDABF trial function. Therefore the metallic $g_{pp}(r)$ at temperature T should correspond to the LDABF $g_{pp}(r)$ at $\sim T/2$. This is indeed observed and the new $g_{pp}(r)$'s from LDABF are in fair agreement with predictions of Car-Parrinello MD.¹⁷ This agreement remains somehow surprising since, beyond the different methods of sampling protonic configurational space, the electronic description in the two methods is quite different. We use LDA orbitals with a backflow transformation and a two body RPA Jastrow while in CPMD, only LDA orbitals are employed. Adding the backflow and the Jastrow we obtain a fair gain of energy and moreover we can improve the bosonic part of the trial function by projecting in imaginary time. Further we strongly reduce the finite size effects by averaging over the undetermined phase of the wave function, while CPMD calculations are performed at the Γ point only for

closed shell systems ($N_p = 54$ and 162). However the final agreement between the two methods indicated that the effects of these improvements on the energy difference is only minor. On the other hand, it is well known in simple liquids that $g(r)$ is not very sensitive to changes of the interaction potential and this might explain the observed agreement.

At lower densities, employing IPP orbitals and RPA Jastrow, we have recently found¹⁶ a continuous molecular dissociation with density, at variance with CPMD which has predicted a first order molecular dissociation transition.¹⁸ The reliability of IPP trial function was only tested on crystal structures and should be further investigated for disordered configurations along the lines shown here. This study is in progress. A recent BOMD study¹⁹ within DFT/GGA has reported a continuous molecular dissociation in agreement with our findings. This agreement suggests that improving the trial functions from IPP to LDABF might change the details of the results but not the overall picture. This confirms that our present method can be most useful in condition where new interesting physics is happening, such as near a liquid-liquid phase transitions or a metallization transition.

Acknowledgments

C.P. acknowledges financial support from MIUR-PRIN2005, D.M.C. and K.T.D. acknowledge support from DOE grant DE-FG52-06NA26170, M.A.M. acknowledges support from a DOE/NNSA-SSS graduate fellowship and M.H. acknowledges support from ACI “Desordre et Interactions Coulombiennes” of French Ministry of Research. D.M.C. and M.H. acknowledge support from a UIUC-CNRS exchange program. Computer time was provided by NCSA and CINECA.

References

1. R. M. Martin, *Electronic Structure. Basic Theory and Practical Methods* (Cambridge University Press, Cambridge, 2004).
2. M. W. C. Foulkes, L. Mitas, R. J. Needs and G. Rajagopal, *Rev. Mod. Phys.* **73**, p. 33 (2001).
3. E. G. Maksimov and Y. I. Silov, *Physics-Uspokhi* **42**, p. 1121 (1999).
4. M. Stadele and R. Martin, *Phys. Rev. Letts.* **84**, 6070 (2000).
5. K. A. Johnson and N. W. Ashcroft, *Nature* **403**, p. 632 (2000).
6. D. Alfé, M. Gillan, M. Towler and R. Needs, *Phys. Rev. B* **70**, p. 161101 (2004).
7. B. L. Hammond, W. A. Lester and P. J. Reynolds, *Monte Carlo methods in Ab Initio Quantum Chemistry* (World Scientific, Singapore, 1994).
8. R. M. Panoff and J. Carlson, *Phys. Rev. Letts.* **62**, p. 1130 (1989).
9. Y. Kwon, D. Ceperley and R. Martin, *Phys. Rev. B* **50**, 1684 (1994).
10. M. Holzmann, D. M. Ceperley, C. Pierleoni and K. Esler, *Phys. Rev. E* **68**, 046707 (2003).
11. P. L. Rios, A. Ma, N. D. Drummond, M. Towler and R. J. Needs, *Phys. Rev. E* **74**, 066701 (2006).
12. J. C. Grossman and L. Mitas, *Phys. Rev. Letts.* **94**, 056403 (2005).
13. S. Sorella and C. Attaccalite, Ab-initio molecular dynamics for high-pressure liquid hydrogen, unpublished, (2007).

14. C. Pierleoni and D. M. Ceperley, *The Coupled Electron-Ion Monte Carlo Method*, in *Computer Simulations in Condensed Matter: from Materials to Chemical Biology*, eds. M. Ferrario, G. Ciccotti and K. Binder, Lecture Notes in Physics, Vol. 703 (Springer-Verlag, 2005), pp. 641–683.
15. C. Pierleoni, D. Ceperley and M. Holzmann, *Phys. Rev. Letts.* **93**, 146402 (2004).
16. K. T. Delaney, C. Pierleoni and D. M. Ceperley, *Phys. Rev. Letts.* **97**, 235702 (2006).
17. J. Kohanoff and J. P. Hansen, *Phys. Rev. E* **54**, p. 768 (1996).
18. S. Scandolo, *Proc. Natl. Acad. Sci. U.S.A.* **100**, p. 3051 (2003).
19. J. Vorberger, I. Tamblyng, B. Militzer and S. A. Bonev, *Phys. Rev. B* **75**, p. 024206 (2007).
20. D. M. Ceperley, M. Dewing and C. Pierleoni, *The Coupled Electron-Ion Monte Carlo Simulation Method*, in *Bridging Times Scales: Molecular Simulations for the Next Decade*, eds. P. Nielaba, M. Mareschal and G. Ciccotti, Lecture Notes in Physics, Vol. 605 (Springer-Verlag, 2002), pp. 473–499.
21. M. Dewing and D. M. Ceperley, *The Coupled Electron-Ion Monte Carlo Simulation Method*, in *Recent advances in Quantum Monte Carlo Methods II*, eds. W. A. Lester, S. M. Rothstein and S. Tanaka (World Scientific, 2002).
22. D. Frenkel and B. Smit, *Understanding Molecular Simulations: From Algorithms to Applications*, 2nd edn. (Academic Press, San Diego, 2002).
23. S. Baroni and S. Moroni, *Reptation quantum Monte Carlo*, in *Quantum Monte Carlo Methods in Physics and Chemistry*, eds. M. Nightingale and C. Umrigar (Kluwer, 1999), p. 313.
24. C. Pierleoni and D. Ceperley, *CHEMPHYSICHEM* **6**, 1872 (2005).
25. D. M. Ceperley and M. Dewing, *J. Chem. Phys.* **110**, p. 9812 (1999).
26. C. Lin, F. H. Zong and D. M. Ceperley, *Phys. Rev. E* **64**, 016702[1] (2001).
27. T. Gaskell, *Proc. Phys. Soc. London* **77**, p. 1182 (1961).
28. D. M. Ceperley and B. J. Alder, *Phys. Rev. B* **36**, p. 2092 (1987).
29. V. D. Natoli, R. M. Martin and D. M. Ceperley, *Phys. Rev. Letts.* **70**, p. 1952 (1993).
30. V. D. Natoli, R. M. Martin and D. M. Ceperley, *Phys. Rev. Letts.* **74**, p. 1872 (1995).
31. M. Payne, M. Teter, D. Allan, T. Arias and J. Joannopoulos, *Rev. Mod. Phys.* **64**, p. 1045 (1992).
32. J. Perdew and A. Zunger, *Phys. Rev. B* **23**, p. 5048 (1981).
33. D. Ceperley and B. Alder, *Phys. Rev. Lett.* **45**, p. 566 (1980).
34. K. T. Delaney and et al., *to be published* .